Replacement of Tyr50 stacked on the si-face of the isoalloxazine ring of the flavin adenine dinucleotide prosthetic group modulates Bacillus subtilis ferredoxin-NADP+ oxidoreductase activity toward NADPH

doi: 10.1007/s11120-015-0099-8

Replacement of Tyr50 stacked on the *si*-face of the isoalloxazine ring of the flavin adenine dinucleotide prosthetic group modulates *Bacillus subtilis* ferredoxin-NADP$^+$ oxidoreductase activity toward NADPH

Daisuke Seo*, Hiroshi Naito, Erika Nishimura, Takeshi Sakurai

Division of Material Science, Graduate School of Natural Science and Technology, Kanazawa University, Kakuma, Kanazawa, Ishikawa 920-1192, Japan

*Corresponding author: Daisuke Seo
Division of Material Science, Graduate School of Natural Science and Technology, Kanazawa University, Kakuma, Kanazawa, Ishikawa 920-1192, Japan
Tel: +81-76-264-5683
Fax: +81-76-264-5742
e-mail: dseo@se.kanazawa-u.ac.jp

Abbreviations:
Fld; flavodoxin, FMN; flavin mononucleotide, FAD; flavin adenine dinucleotide, Fd; ferredoxin, FNR; ferredoxin-NAD(P)$^+$ oxidoreductase, G6P; glucose-6-phosphate, G6PDH; glucose-6-phosphate dehydrogenase, HEPES; 4-(2-hydroxyethyl)-1-piperazineethanesulfonic acid, K_d; dissociation constant, K_m; Michaelis constant, SDS-PAGE; sodium dodecyl sulfate-polyacrylamide gel electrophoresis, TrxR; bacterial NADPH-thioredoxin reductase, WT; wild type.

Keywords: ferredoxin, flavin adenine dinucleotide, NADPH, tyrosine

Abstract

Ferredoxin-NAD(P)$^+$ oxidoreductases ([EC 1.18.1.2], [EC 1.18.1.3], FNRs) from green sulfur bacteria, purple non-sulfur bacteria and most of Firmicutes such as *Bacillus subtilis* (*Bs*FNR) are homo-dimeric flavoproteins homologous to bacterial NADPH-thioredoxin reductase. These FNRs contain two unique aromatic residues stacked on the *si*- and *re*-face of the isoalloxazine ring moiety of the FAD prosthetic group whose configurations are often found among other types of flavoproteins including plant-type FNR and flavodoxin, but not in bacterial NADPH-thioredoxin reductase. To investigate the role of the *si*-face Tyr50 residue in *Bs*FNR, we replaced Tyr50 with Gly, Ser and Trp and examined its spectroscopic properties and enzymatic activities in the presence of NADPH and ferredoxin (Fd) from *B. subtilis* (*Bs*Fd).

The replacement of Tyr50 to Gly (Y50G), Ser (Y50S) and Trp (Y50W) in *Bs*FNR resulted in a blue shift of the FAD transition bands. The Y50G and Y50S mutations enhanced the FAD fluorescence emission whereas those of the wild type and Y50W mutant were quenched. All three mutants decreased thermal stabilities compared to wild type. Using a diaphorase assay, the k_{cat} values for the Y50G and Y50S mutants in the presence of NADPH and ferricyanide were decreased to less than 5% of the wild type activity. The Y50W mutant retained approximately 20% reactivity in the diaphorase assay and *Bs*Fd-dependent cytochrome *c* reduction assay relative to wild type. The present results suggest that Tyr50 modulates the electronic properties and positioning of the prosthetic group.

Introduction

Ferredoxin-NAD(P)$^+$ oxidoreductase ([EC 1.18.1.2], [EC 1.18.1.3], FNR), catalyze the redox reaction between the two electron carrier nucleotide NAD(P)$^+$/H and the small electron transfer proteins containing the iron-sulfur cluster(s), ferredoxin (Fd), or the flavin mononucleotide (FMN), flavodoxin (Fld).

$$NADPH + 2Fd_{ox} \text{ (or } 2Fld_{ox}) + H^+ \leftrightarrows NADP^+ + 2Fd_{red} \text{ (or } 2Fld_{red}) \quad (1)$$

Fd is ubiquitous in almost all organisms, functioning as an electron mediator in cytochrome P450 dependent hydroxylation, nitrogen assimilation, and NADP$^+$ reduction from reduced Fd during photosynthesis (Aliverti et al. 2008; Ceccarelli et al. 2004; Munro et al. 2007; Knaff and Hirasawa 1991; Ewen et al. 2011). FNR, a member of the flavoprotein superfamily, contains a flavin adenine dinucleotide (FAD) or rarely, FMN as the prosthetic group. In the process catalyzed by FNRs (Eq. 1), a hydride transfer reaction with NAD(P)H and two separate one-electron transfer reactions with Fd are generally involved. These reactions occur via the formation of competent FNR-substrate complexes with NAD(P)H and Fd. For the redox reactions to occur with a rapid turnover rate, appropriate positioning of the cofactors and reacting atoms/groups for hydride and electron tunneling in the complexes, and tuning of the redox properties of the redox centers are required (Moser et al. 2010). In this sense, comparative studies of the different types of FNRs should contribute to increasing our understanding of the structure-function relationship of FNRs.

FNRs are structurally and phylogenetically classified into two unrelated families including five subgroups (Aliverti et al. 2008; Dym and Eisenberg 2001; Correll et al. 1993; Karplus and Faber 2004;

Seo et al. 2004; Muraki et al. 2010). Phylogenetic analyses of the deduced amino acid sequences (Seo et al. 2004) and crystal structures of FNRs from the green sulfur bacterium *Chlorobaculum tepidum* (Muraki et al. 2010), the low GC gram positive bacterium *Bacillus subtilis* (*Bs*FNR, Komori et al. 2010) and thermophile *Thermus thermophiles* (PDB code; 2ZBW) have revealed that these FNRs are homologous to the NADPH-dependent bacterial thioredoxin reductase (TrxR) from *Escherichia coli* (*Ec*TrxR) (Waksman et al. 1994), referred as a TrxR-type FNR. The deduced genes of TrxR-type FNR are distributed among most of Firmicutes except for clostridia and heliobacteria, several alpha-proteobacteria including purple non-sulfur bacteria, green sulfur bacteria, and several archaea. Phylogenetic analysis of FNRs in prokaryotes revealed that the amino acid sequences of Fd and FNR from green sulfur bacteria and cyanobacteria are phylogenetically unrelated (Seo et al. 2002), although both utilize Fd and FNR in $NAD(P)^+$ photoreduction process. Interestingly, purple sulfur bacteria possess a plant-type FNR and [2Fe-2S] type Fd, but the photosynthetic reaction center of the bacteria cannot reduce Fd directly. Comparative studies of FNRs from different organisms including photosynthetic and non-photosynthetic ones would provide important information on origin and evolution of photosynthesis in addition to the structure-function relationships.

TrxR-type FNR is unique among FNRs for its homo-dimer form and having the C-terminal extension which covers the *re*-face of the isoalloxazine ring of the other protomer (Fig. 1a). In the crystal structures of TrxR-type FNR, two aromatic residues are stacked on the *si*- and *re*-face of the isoalloxazine ring moiety of the FAD prosthetic group. The *re*-face aromatic residue in the C-terminal extension is Phe in green sulfur bacterial FNR, His in FNRs from most heterotrophs including *Bs*FNR, and Tyr in purple non-sulfur bacterial FNR, whereas the *si*-face Tyr is highly conserved (Fig. 1b). In the crystal structure of *Bs*FNR (Komori et al. 2010), Tyr50 on the *si*-face and His324 on the *re*-face of

the isoalloxazine ring moiety stacked almost in parallel to the isoalloxazine ring moiety at a distance of approximately 3.3–3.6 Å (Fig. 1a). In the structure of *Ec*TrxR (Waksman et al. 1994), both of the corresponding aromatic residues are missing (Fig. 1b), indicating importance in the functional role of FNR. Interestingly, aromatic residues are often found on both sides of the isoalloxazine ring moiety of the FAD prosthetic group among the plant-type FNR superfamily and Fld. Mutational analyses have shown that replacement of the *si*-face Tyr residues in the FNRs from pea and cyanobacteria (Arakaki et al. 2001; Sánchez-Azqueta et al. 2014), and cytochrome b_5 reductase (Cytb_5R, Marohnic et al. 2005) changed the spectroscopic, catalytic and thermodynamic properties of the proteins. In the case of flavodoxins from *Desulfovibrio vulgaris* and *Anabaena* PCC7119, the *si*-face Tyr plays a role in adjusting the stability of the prosthetic group in different redox states (Swenson and Krey 1994; Lostao et al. 1997).

Previously, the depletion of the C-terminal extension region of *Bs*FNR, including the *re*-face His324 residue, significantly decreased the reduction rate of *Bs*Fd and slightly enhanced the catalysis with NAD(P)H (Seo et al. 2014). Replacement of the *re*-face His324 in *Bs*FNR (Komori et al. 2010) and *Ct*FNR (Muraki et al. 2010) did not significantly affect the reactivity and selectivity toward NAD(P)H. These results are in contrast to the reports on the role of the corresponding residues on the *re*-face of the isoalloxazine ring moiety in the plant-type FNR super families (Piubelli et al. 2000; Nogues et al. 2004; Tejero et al. 2005; Neeli et al. 2005; Baroni et al. 2012). Herein, we report the replacement of the *si*-face Tyr50 residue in TrxR-type *Bs*FNR to Trp, Ser and Gly, and the resulting effects on the spectroscopic and enzymatic properties by steady-state reaction analyses. By replacing Tyr50 with the nonaromatic Gly and Ser residues, the reactivity toward NADPH was drastically decreased, whereas the reactivity toward NADPH and *Bs*Fd reduction were retained by replacement

with the Trp residue.

Materials and Methods

Preparations of BsFNR and its mutants, and B. subtilis Fd

Expression vectors for the mutations of *Bs*FNRs were prepared by the Quikchange method with the expression vector for wild type (WT) enzyme as the template (Seo et al. 2014) and following primers: Y50G Fwd (5′ GCC CTA GGC CCT GAG AAG TAT ATA TAT GAT GTA GCG 3′), Y50G Rev (5′ CTC AGG GCC TAG GGC GCT AAG CTG TCC G), Y50W Fwd (5′ GCC CTA TGG CCT GAG AAG TAT ATA TAT GAT GTA GCG 3′), Y50W Rev (5′ CTC AGG CCA TAG GGC GCT AAG CTG TCC G 3′), Y50S Fwd (5′ GGA CAG CTT AGC GCC CTA AGC CCT GAG AAG TAT ATA 3′), Y50S Rev (5′ TAT ATA CTT CTC AGG GCT TAG GGC GCT AAG CTG TCC 3′), Y50F Fwd (5′ GGA CAG CTT AGC GCC CTA TTC CCT GAG AAG TAT ATA 3′), Y50F Rev (5′ TAT ATA CTT CTC AGG GAA TAG GGC GCT AAG CTG TCC 3′). The DNA sequence of the open reading frame of the mutated *Bs*FNR genes in the plasmid was verified by DNA sequencing (Hitachi SQ5500, Tokyo, Japan). The resulting plasmid was transformed into Tuner(DE3)pLacI cells (Novagen, Merck Millipore). Expression and purification of WT and mutated *Bs*FNRs were performed according to the methods for WT *Bs*FNR (Seo et al. 2014). *B. subtilis* Fd was prepared according to Seo et al. (2009, 2014).

Spectroscopic analyses

The UV-visible absorption spectra were measured with a double beam spectrophotometer (V-560, JASCO) in 20 mM 4-(2-hydroxyethyl)-1-piperazineethanesulfonic acid (HEPES)-NaOH buffer (pH 7.0) at room temperature, as described previously (Seo et al. 2014). Difference spectra were obtained by subtracting the control spectrum recorded prior to the addition of substrates from the experimentally

obtained spectra after correcting for volume changes using 9-10 μM *Bs*FNR solution. K_d values were determined according to the method described in the previous study (Batie and Kamin 1984, Seo et al. 2014).

Fluorescence spectra of the oxidized *Bs*FNRs and FAD were measured on a fluorescence spectrometer (Hitachi F-4500) at room temperature. FAD was purchased from Sigma-Aldrich Japan. Thermal stabilities of the WT and mutated *Bs*FNRs in oxidized form were examined essentially according to Marohnic et al (2005). *Bs*FNR solution (9-10 μM) in 20 mM HEPES-NaOH buffer was incubated at each temperature in a range from 20 to 90°C for 5 min then cooled on ice. After 20 min centrifugation at 16,000×g, supernatant was retained. Fluorescence intensity with excitation at 450 nm and emission at 525 nm of the supernatant was measured on a fluorescence spectrophotometer (Hitachi F-2500).

Steady state enzyme assays

The NAD(P)H diaphorase assay using 3 mM potassium ferricyanide as an electron acceptor and the NADPH-dependent cytochrome *c* reduction assay in the presence or absence of Fd from *B. subtilis* (*Bs*Fd) were performed in 20 mM HEPES-NaOH buffer (pH 7.0) at 25°C under aerobic conditions essentially as described previously (Seo et al. 2014). Turnover rates were calculated by subtracting the respective assay blank containing all reagents except for the FNRs. K_m and k_{cat} values were determined by a nonlinear regression analysis using the Michaelis–Menten equation with IgorPro software (ver. 6.3, WaveMetrics, USA). Turnover rates are expressed as the number of NADPH molecules consumed by one molecule of native-form FNR.

Protein subunit and substrate concentrations were determined using the extinction coefficients

for WT *Bs*FNR (ε_{457} = 12.3 mM^{-1} cm^{-1}) (Seo et al. 2004), Y50G and Y50S mutants (ε_{457} = 12.7 mM^{-1} cm^{-1}), Y50W mutant (ε_{458} = 11.8 mM^{-1} cm^{-1}), *Bs*Fd (ε_{390} = 16.0 mM^{-1} cm^{-1}) (Green et al. 2003), potassium ferricyanide (ε_{420} = 1.02 mM^{-1} cm^{-1}) and NADPH (ε_{340} = 6.2 mM^{-1} cm^{-1}).

Miscellaneous methods

Sodium dodecyl sulfate-polyacryl amide gel electrophoresis (SDS-PAGE) analysis was performed as described by Laemmli (1970). Protein bands on a 12% gel were visualized with Coomassie Brilliant Blue R-250.

Absorption coefficients for WT and mutated *Bs*FNRs were determined by the heat denaturation method using the extinction coefficient of FAD in a neutralized supernatant (11.3 $mM^{-1}cm^{-1}$ at 450 nm) (Aliverti et al. 1999).

The apparent molecular masses of WT and mutated *Bs*FNRs were estimated by gel-permeation chromatography as described (Seo et al. 2009, 2014).

Results

Preparation of mutated FNRs and investigation of their spectroscopic properties

Three *Bs*FNR mutants, Y50G, Y50S and Y50W, were purified to apparent homogeneity using the method for the recombinant WT enzyme (Fig. 2a). Expression and purification of the Y50F mutant was not successful, likely because of low expression in the soluble fraction and/or it was unstable under the experimental conditions. The molecular mass of the mutated *Bs*FNR polypeptides of Y50G, Y50S and Y50W migrated with an apparent molecular mass of 40 kDa on SDS-PAGE (Fig. 2a) and eluted as a single peak during gel-permeation chromatography exhibiting similar apparent molecular masses as WT (data not shown).

The UV-visible absorption spectra of Y50G and Y50S mutants exhibited a blue shift of the FAD transition band II with peak at 374 nm and a decrease in absorption coefficient of the shoulder around 490 nm compared with WT (Fig. 2b). Absorption coefficients of Y50G and Y50S *Bs*FNRs in both band regions slightly increased compared with those of WT (Fig. 2b, Table 1). The FAD transition band II of Y50W with peak at 375 nm also blue shifted compared with those of WT. The FAD transition band I appears to broaden (Fig. 2b, dashed line). In the equivalent Fld mutants, a long-wavelength band extending from 500 nm to 700 nm was assigned as a charge transfer band (Swenson and Krey 1994; Lostao et al. 1997). In contrast to WT and the other mutants, the absorption coefficients of the FAD transition band II of the Y50W mutant were significantly decreased (Fig. 2b).

Addition of $NADP^+$ to the FNR solution induced changes in the FAD transition bands with peaks at 470 and 505–513 nm, and troughs at 450–456 and 478–483 nm on the difference spectra (Fig. 2c). The difference spectra of the Y50G and Y50S mutants were very similar although the slope beyond 510 nm is small when compared with that of WT *Bs*FNR. In contrast, the slope of the Y50W mutant

was broad beyond 520 nm in the difference spectra, which seemed to be related to the broadening observed in the UV-vis absorption spectrum (Fig. 2b). Plots of the absorption change (ΔA_{510-4} minus ΔA_{485-7}) against $NADP^+$ concentration provided saturation curves. The K_d values of the Y50G and Y50S mutants decreased to less than half that of WT *Bs*FNR (Table 1), whereas the K_d value of Y50W was similar to that of WT.

The fluorescence intensity of the protein-bound FAD is influenced by its environment (Heelis 1982; Yagi et al. 1980). The fluorescence emissions of Y50G and Y50S increased 6- to 7-fold compared with that of free FAD, whereas the fluorescence emission of WT and Y50W *Bs*FNRs were efficiently quenched to < 3% and 9% of that of free FAD (Fig. 3a). In the crystal structure of *Bs*FNR (Komori et al. 2010), the FAD prosthetic group is noncovalently bound in the open conformation. The absence of the Tyr aromatic residue could explain the enhancement of the fluorescence emission in the Y50G and Y50S mutants whereas the low emission of the Y50W mutant indicated that the substituted Trp residue in the Y50W mutant interacted with the isoalloxazine ring (Heelis 1982).

Influence of the Tyr50 substitution on the thermal stability was examined by measuring the flavin fluorescence emissions of the retained supernatant after incubation (Fig. 3b). The T_m values which provide 50% of maximum difference fluorescence intensity of all mutated *Bs*FNRs were in a range of 40 to 50 °C which is about 20°C lower than that of WT, indicating Tyr50 play an important role to stabilize the FAD prosthetic group.

Steady-state reactions of BsFNR with NADPH and ferredoxin

To evaluate the reactivity of the mutated *Bs*FNRs with NADPH, the diaphorase assay was performed using potassium ferricyanide as the electron acceptor (Table 1). Upon replacement of Tyr50

with the nonaromatic residues Gly and Ser, the k_{cat} values drastically decreased to 4.2% and 1.6%, respectively, of that of WT *Bs*FNR (Table 1). Although the k_{cat} value for the Y50W mutant *Bs*FNR was also decreased to 18% of that of WT, its k_{cat}/K_m value was close to that of WT (Table 1).

To evaluate the Fd reduction rate catalyzed by FNR under steady-state reaction conditions, a cytochrome *c* reduction assay was performed using cytochrome *c* as the final electron acceptor (Fig. 4). Under the assay conditions, the cytochrome *c* reduction rate affects the Fd-independent cytochrome *c* reduction rate by FNRs, which could be estimated from the rate obtained in the absence of *Bs*Fd (Fig. 4). Similar to WT, mutated *Bs*FNRs exhibited relatively low direct cytochrome *c* reduction rates. The cytochrome *c* reduction rate of the Y50G and Y50S mutants did not increase with an increase in the *Bs*Fd concentration, whereas the reduction rate of the Y50W mutant substantially increased as the Fd concentration increased, indicating the Y50W mutant retained *Bs*Fd reduction activity. Because the reducing equivalents are supplied by NADPH in this assay, the slow rate of donation from NADPH for the Y50G and Y50S mutants observed in the diaphorase assay could be one of the reasons for the low cytochrome *c* reduction rate in the *Bs*Fd dependent cytochrome *c* reduction assay.

Discussion

Replacement of the *si*-face Tyr50 in *Bs*FNR significantly affected its spectroscopic and enzymatic properties. The $NADP^+$ binding mode observed in the crystal structures of *Bs*FNR and *Ec*TrxR (Komori et al. 2010; Waksman et al. 1994; Lennon et al. 2000) indicated the nicotinamide ring of $NADP^+$/H would access the *re*-face of the isoalloxazine ring during the hydride transfer process. The *si*-face Tyr50 residue may alter the reactivity of *Bs*FNR toward NADPH by modulating the localization and/or redox properties of the FAD prosthetic group and/or the protein conformation. This is in contrast to the *re*-face residues that could directly interact with the nicotinamide moiety of $NADP^+$/H (Seo et al. 2014).

Replacement of the aromatic Tyr50 residue with the nonaromatic Gly and Ser residues induced the blue shift of the FAD transition bands and enhancement of the fluorescence emission (Fig. 2b, c, Fig. 3a). These changes have been reported to be due to the modification in the environment around the isoalloxazine ring, a decrease in the number of hydrogen bonds and the loss of hydrophobic stacking with the aromatic residue (Heelis 1982; Yagi et al. 1980). Although the replacements of Tyr50 disrupted the hydrogen bond between the O2′ hydroxyl group of the ribityl moiety of FAD and the hydroxyl group of the Tyr residue (Fig. 1a), the impact of the depletion of this hydrogen bond on the spectroscopic properties are uncertain (Heelis 1982). Truncation of the C-terminal region of *Bs*FNR including the Ser325 residue known to form a hydrogen bond to the O4 atom of the isoalloxazine ring moiety induced the blue shift in the absorption spectrum (Komori et al. 2010; Seo et al. 2014). Analogous mutations performed on Cytb_5R also induced a blue shift of the transition band and an enhancement of fluorescence emission (Marohnic et al. 2005). The observed low fluorescence emission suggests that the Trp50 residue in Y50W *Bs*FNR is located close enough to the isoalloxazine

ring moiety to participate in hydrophobic stacking as observed for WT *Bs*FNR. This close contact of the aromatic amino acid residues with the isoalloxazine ring has been described as the dominant force responsible for the observed fluorescent quenching (Heelis 1982). The blue shift and decrease in the intensity of the FAD transition band II would have results for a more apolar environment induced by the bulky Trp (Heelis, 1982; Müller et al. 1973).

The spectroscopic data for the *Bs*FNR mutants are in accordance with the previous results for the analogous mutants in the plastid-type FNR superfamilies and Flds. Replacements of Tyr50 in *Bs*FNR also lowered the diaphorase activity as reported in the analogous mutations of the plant-type FNR superfamily, although the extent of decrease differed between *Bs*FNR and plant-type FNR superfamily. In Cytb_5R and plant-type FNR, the centroid of pyrimidine ring of isoalloxazine ring and phenol ring of the Tyr residue is distant ~5 Å (Arakai et al. 2001; Marohnic et al. 2005). The hydroxyl group of Tyr residue is hydrogen-bonded with the O4' hydroxyl group of the ribityl moiety in FAD prosthetic group. Mutation of Tyr79 to Phe in *An*FNR did not result in any significant modification of the FAD isoalloxazine environment (Sánchez-Azqueta et al. 2014). In pea FNR, it appeared as if there was no space to accommodate the bulky Trp side-chain (Arakaki et al. 2001). In *Bs*FNR, Tyr50 is positioned in the long flexible loop and its side chain is stacked on the dimethylbenzene ring of the isoalloxazine ring in the crystal structure. There appears to be a space to accommodate the bulky side-chain of Trp (Fig. 1a). In general, hydride transfer requires closer contact between the donor-acceptor atoms or groups than electron transfer (Moser et al. 2010). In the crystal structure of *Bs*FNR, the distance between the centroid of the side-chain of Tyr50 and the isoalloxazine ring is closer than that of plant-type FNR superfamily (3.4 Å in *Bs*FNR, Komori et al. 2010). The loss of the hydrogen bond between the hydroxyl group of Tyr50 and the O2′ hydroxyl group of the ribityl moiety of FAD and and π-π

interaction between two rings significantly perturbs the location of the isoalloxazine ring moiety during the *Bs*FNR catalyzed reaction, which would decrease the k_{cat}/K_m values of the Y50G and Y50S mutants. In contrast to the reaction with NADPH, the reduction rates of the protein partners were decreased by the replacement of the *si*-face Tyr to Trp in *Bs*FNR and Cytb_5R (Marohnic et al. 2005). As proposed for *An*FNR (Sánchez-Azqueta et al. 2014) and reported in the corresponding studies on Flds (Swenson and Krey 1994), *si*-face Tyr residues are likely involved in regulating the redox properties. We could not determine the redox potential of *Bs*FNR by the titration method with dithionite in the presence of small amount of mediators (neutral red, benzyl viologen and methyl viologen). We will report details of the redox properties of *Bs*FNR elsewhere.

Acknowledgement

We gratefully thank Profs. Hitoshi Tamiaki and Tadashi Mizoguchi at Ritsumeikan University for their help with the measurements of fluorescence spectra.

References

Aliverti A, Pandini V, Pennati A, de Rosa M, Zanetti G (2008) Structural and functional diversity of ferredoxin-NADP$^+$ reductases. Arch Biochem Biophys 474:283-291

Aliverti A, Curti B, Vanoni MA (1999) Identifying and quantitating FAD and FMN in simple and in iron-sulfur-containing flavoprotein. In: Chapman SK, Reid GA (eds) Flavoprotein Protocols, Vol. 131. Methods in Molecular Biology. Humana Press, Totowa, New Jersey, USA, pp 9-23.

Arakaki AK, Orellano EG, Calcaterra NB, Ottado J, Ceccarelli EA (2001) Involvement of the flavin *si*-face tyrosine on the structure and function of ferredoxin-NADP$^+$ reductases. J Biol Chem 276:44419-44426

Baroni S, Pandini V, Vanoni MA, Aliverti A (2012) A single tyrosine hydroxyl group almost entirely controls the NADPH specificity of *Plasmodium falciparum* ferredoxin-NADP$^+$ reductase. Biochemistry 51:3819-3826

Batie CJ, Kamin H (1984) Ferredoxin:NADP$^+$ oxidoreductase. Equilibria in binary and ternary complexes with NADP$^+$ and ferredoxin. J Biol Chem 259:8832-8839

Bianchi V, Reichard P, Eliasson R, Pontis E, Krook M, Jornvall H, Haggard-Ljungquist E (1993) *Escherichia coli* ferredoxin NADP$^+$ reductase: Activation of *E. coli* anaerobic ribonucleotide reduction, cloning of the gene (*fpr*), and overexpression of the protein. J Bacteriol 175:1590-1595

Ceccarelli EA, Arakaki AK, Cortez N, Carrillo N (2004) Functional plasticity and catalytic efficiency in plant and bacterial ferredoxin-NADP(H) reductases. Biochim Biophys Acta 1698:155-165

Correll CC, Ludwig ML, Bruns CM, Karplus PA (1993) Structural prototypes for an extended family

of flavoprotein reductases: comparison of phthalate dioxygenase reductase with ferredoxin reductase and ferredoxin. Protein Sci 2:2112-2133

Dym O, Eisenberg D (2001) Sequence-structure analysis of FAD-containing proteins. Protein Sci 10:1712-1728

Ewen KM, Kleser M, Bernhardt R (2011) Adrenodoxin: The archetype of vertebrate-type [2Fe-2S] cluster ferredoxins. Biochim Biophys Acta 1814:111-125

Green AJ, Munro AW, Cheesman MR, Reid GA, Von Wachenfeldt C, Chapman SK (2003) Expression, purification and characterisation of a *Bacillus subtilis* ferredoxin: A potential electron transfer donor to cytochrome P450 BioI. J Inor Biochem 93:92-99

Heelis PF (1982) The photophysical and photochemical properties of flavins (isoalloxazines). Chemical Society Reviews 11:15-39

Karplus PA, Faber HR (2004) Structural aspects of plant ferredoxin: $NADP^+$ oxidoreductases. Photosyn Res 81:303-315

Knaff DB, Hirasawa M (1991) Ferredoxin-dependent chloroplast enzymes. Biochim Biophys Acta 1056:93-125

Komori H, Seo D, Sakurai T, Higuchi Y (2010) Crystal structure analysis of *Bacillus subtilis* ferredoxin-$NADP^+$ oxidoreductase and the structural basis for its substrate selectivity. Protein Sci 19:2279-2290

Laemmli UK (1970) Cleavage of structural proteins during the assembly of the head of bacteriophage T4. Nature 227:680-685

Lennon BW, Williams Jr CH, Ludwig ML (2000) Twists in catalysis: alternating conformations of *Escherichia coli* thioredoxin reductase. Science 289:1190-1194

Lostao A, Gomez-Moreno C, Mayhew SG, Sancho J (1997) Differential stabilization of the three FMN redox forms by tyrosine 94 and tryptophan 57 in flavodoxin from *Anabaena* and its influence on the redox potentials. Biochemistry 36:14334-14344

Marohnic CC, Crowley LJ, Davis CA, Smith ET, Barber MJ (2005) Cytochrome b_5 reductase: role of the *si*-face residues, proline 92 and tyrosine 93, in structure and catalysis. Biochemistry 44:2449-2461

Moser CC, Ross Anderson JL, Dutton PL (2010) Guidelines for tunneling in enzymes. Biochim Biophys Acta 1797:1573-1586

Müller F, Mayhew SG, Massey V (1973) On the effect of temperature on the absorption spectra of free and protein-bound flavine. Biochemistry 12:4654-4662

Munro AW, Girvan HM, McLean KJ (2007) Cytochrome P450-redox partner fusion enzymes. Biochim Biophys Acta 1770:345-359

Muraki N, Seo D, Shiba T, Sakurai T, Kurisu G (2010) Asymmetric dimeric structure of ferredoxin-NAD(P)$^+$ oxidoreductase from the green sulfur bacterium *Chlorobaculum tepidum*: implications for binding ferredoxin and NADP$^+$. J Mol Biol 401:403-414

Neeli R, Roitel O, Scrutton NS, Munro AW (2005) Switching pyridine nucleotide specificity in P450 BM3: mechanistic analysis of the W1046H and W1046A enzymes. J Biol Chem 280:17634-17644

Nogués I, Tejero J, Hurley JK, Paladini D, Frago S, Tollin G, Mayhew SG, Gómez-Moreno C, Ceccarelli EA, Carrillo N, Medina M (2004) Role of the C-terminal tyrosine of ferredoxin-nicotinamide adenine dinucleotide phosphate reductase in the electron transfer processes with its protein partners ferredoxin and flavodoxin. Biochemistry 43:6127-6137

Pettersen EF, Goddard TD, Huang CC, Couch GS, Greenblatt DM, Meng EC, Ferrin TE (2004) UCSF Chimera--a visualization system for exploratory research and analysis. J Comput Chem 25: 1605-1612.

Piubelli L, Aliverti A, Arakaki AK, Carrillo N, Ceccarelli EA, Karplus PA, Zanetti G (2000) Competition between C-terminal tyrosine and nicotinamide modulates pyridine nucleotide affinity and specificity in plant ferredoxin-$NADP^+$ reductase. J Biol Chem 275:10472-10476

Sánchez-Azqueta A, Herguedas B, Hurtado-Guerrero R, Hervás M, Navarro JA, Martínez-Júlvez M, Medina M (2014) A hydrogen bond network in the active site of *Anabaena* ferredoxin-NADP($^+$) reductase modulates its catalytic efficiency. Biochim Biophys Acta 1837:251-263

Seo D, Sakurai H (2002) Purification and characterization of ferredoxin-$NAD(P)^+$ reductase from the green sulfur bacterium *Chlorobium tepidum*. Biochim Biophys Acta 1597:123-132

Seo D, Kamino K, Inoue K, Sakurai H (2004) Purification and characterization of ferredoxin-$NADP^+$ reductase encoded by *Bacillus subtilis yumC*. Arch Microbiol 182:80-89

Seo D, Okabe S, Yanase M, Kataoka K, Sakurai T (2009) Studies of interaction of homo-dimeric ferredoxin-$NAD(P)^+$ oxidoreductases of *Bacillus subtilis* and *Rhodopseudomonas palustris*, that are closely related to thioredoxin reductases in amino acid sequence, with ferredoxins and pyridine nucleotide coenzymes. Biochim Biophys Acta 1794:594-601

Seo D, Asano T, Komori H, Sakurai T (2014) Role of the C-terminal extension stacked on the *re*-face of the isoalloxazine ring moiety of the flavin adenine dinucleotide prosthetic group in ferredoxin-NADP($^+$) oxidoreductase from *Bacillus subtilis*. Plant Physiol Biochem 81:143-148

Swenson RP, Krey GD (1994) Site-directed mutagenesis of tyrosine-98 in the flavodoxin from *Desulfovibrio vulgaris* (Hildenborough): regulation of oxidation-reduction properties of the

bound FMN cofactor by aromatic, solvent, and electrostatic interactions. Biochemistry 33:8505-8514

Tejero J, Perez-Dorado I, Maya C, Martinez-Julvez M, Sanz-Aparicio J, Gómez-Moreno C, Hermoso JA, Medina M (2005) C-terminal tyrosine of ferredoxin-$NADP^+$ reductase in hydride transfer processes with $NAD(P)^+$/H. Biochemistry 44:13477-13490

Waksman G, Krishna TS, Williams Jr CH, Kuriyan J (1994) Crystal structure of *Escherichia coli* thioredoxin reductase refined at 2 Å resolution. Implications for a large conformational change during catalysis. J Mol Biol 236:800-816

Yagi K, Ohishi N, Nishimoto K, Choi JD, Song PS (1980) Effect of hydrogen bonding on electronic spectra and reactivity of flavins. Biochemistry 19:1553-1557

Figure legends

Figure 1 (a) Close-up view around the isoalloxazine ring moiety of the FAD prosthetic group in the crystal structure of *Bs*FNR (PDB code: 3LZX) and *Ec*TrxR (PDB code; 1TDE). Main chains of subunits A including the FAD prosthetic group, and subunit B in *Bs*FNR are colored in red and blue, respectively. Main chain of the residues from 1 to 113 and the FAD prosthetic group in *Ec*TrxR are colored in green. Side chains of Tyr50 in subunit A and His324 in subunit B of *Bs*FNR are depicted as a ball and stick model. Hydrogen-bonding between Tyr50 and O2' hydroxyl group of ribitol moiety of FAD in *Bs*FNR is depicted as a dotted line. Superposition of the main chain of *Ec*TrxR from 1 to 113 with *Bs*FNR was performed using the UCSF Chimera package (Pettersen et al. 2004). The figure was prepared using Discovery Studio 4.0 Visualizer (Accelrys Inc., USA). (b) Partially aligned amino acid sequences around the *si*-face residues in TrxR-type FNRs and TrxRs. The numbers of the amino acid residues in *Bs*FNR are indicated in the upper line. The position of the Tyr50 residue in the *Bs*FNR sequence is indicated by an arrow. The positions of the 2nd and 3rd helices assigned in the crystal structure of *Bs*FNR (Komori et al. 2010) and corresponding secondary structure in *Ec*TrxR (Waksman et al. 1994) are indicated by the rods in the upper and bottom lines, respectively. bsu_yumC: *Bacillus subtilis* subsp. *subtilis str. 168* FNR (this work), rpa_RPA3954: *Rhodopseudomonas palustris* CGA009 FNR, cte_CT1512: *Chlorobaculum tepidum* FNR, eco_trxB: *Escherichia coli* K12 TrxR, bsu_trxB: *B. subtilis* subsp. *subtilis str. 168* TrxR.

Figure 2 (a) SDS-PAGE of WT *Bs*FNR (Lane 2), Y50G (Lane 3), Y50S (Lane 4) and Y50W (Lane 5) mutants with CBB staining. Each lane contained 40-50 pmol *Bs*FNRs. Lane 1; molecular mass

markers (250, 150, 100, 75, 50, 37, 25, 20, 15 kDa from upside).

(b) UV-visible absorption spectra of mutated *Bs*FNRs in the air-oxidized form. The spectra of approximately 9 μM *Bs*FNRs in 20 mM HEPES-NaOH buffer (pH 7.0) were measured at room temperature. Absorption coefficients of *Bs*FNRs were estimated based on the FAD concentration as described in Materials and Methods section. Thick continuous line: Y50G, dotted line: Y50S, dashed line Y50W. The spectrum of WT enzyme (thin solid line) was obtained from Seo et al. (2014). (c) Difference spectra induced by addition of 1 mM $NADP^+$. Measurements were performed at room temperature in 20 mM HEPES-NaOH buffer (pH 7.0). Thick continuous line; Y50G, dotted line: Y50S, dashed line: Y50W. The spectrum of WT *Bs*FNR (thin solid line) was obtained from Seo et al. (2014).

Figure 3 (a) Fluorescence emission spectra of WT and mutated *Bs*FNRs. The fluorescence of the solution containing 3.4–5.1 μM FAD in 20 mM HEPES-NaOH buffer was measured at room temperature. Fluorescence intensities were normalized to that obtained for a FAD concentration of 5 μM. Emission spectra of free FAD (thin solid line), WT (dot-dash line), Y50G (thick solid line), Y50S (dotted line), Y50W (dashed line) were measured from 460–700 nm with excitation at 450 nm. (b) Thermal stability profiles of air oxidized WT (○), Y50G (●), Y50S (■) and Y50W (▲) *Bs*FNRs. The supernatant (9-10 μM *Bs*FNR) after incubation at indicated temperature for 5 min followed by centrifugation was retained. Fluorescence intensity of the diluted supernatant (4-5 μM FAD) with excitation at 450 nm and emission at 525 nm was measured. The fluorescence intensities are normalized by subtracting the intensity at 20°C for WT and Y50W, or at 90°C for Y50G and Y50S, and dividing by the difference intensity between 20°C and 90°C. Each data is average of three measurement.

Figure 4 Effect of Fd concentration on the cytochrome *c* reduction of Y50G (●), Y50S (■) and Y50W (▲) *Bs*FNR mutants. The assays were performed in 20 mM HEPES-NaOH buffer (pH 7.0) at 25°C. Reaction mixtures contained 5 mM glucose-6-phosphate, 5 U ml^{-1} glucose-6-phosphate dehydrogenase, 0.1 mM horse heart cytochrome *c*, 5 μM NADPH and 10–20 nM *Bs*FNRs with or without *B. subtilis* Fd as indicated. Observed rates are obtained by subtraction of the respective assay blank containing all the assay reagents except the FNR. Each data point was the average of three measurements. Error bars represent ± one standard deviations. The data set of WT *Bs*FNR (○) was obtained from Seo et al. (2014).

Table 1 Enzymatic and spectroscopic properties of WT and Y50 mutants

	WT	Y50G	Y50S	Y50W
NADPH diaphorase (ferricyanide)[a]				
K_m for NADPH (μM)	19.7 ± 0.5	4.3 ± 0.4	1.9 ± 0.2	4.0 ± 0.3
k_{cat} (s^{-1})	1012 ± 6	42.8 ± 1.0	16.2 ± 0.4	183 ± 3
k_{cat} / K_m ($s^{-1}M^{-1}$)	5.1×10^7	1.0×10^7	8.5×10^6	4.6×10^7
NADH diaphorase (ferricyanide) (s^{-1})	1.4 ± 0.4[b]	< 1 s^{-1}[c]	< 1 s^{-1}[c]	< 1 s^{-1}[c]
K_d for $NADP^+$ (μM)	4.6 ± 0.2[d]	1.8 ± 0.6	1.1 ± 0.6	6.5 ± 1.7
ε ($mM^{-1}cm^{-1}$ FAD^{-1}) / at λ max (nm)	12.3/ 457[e]	12.7/ 457	12.7/ 457	11.8/458

a: at 3 mM ferricyanide

b: at 3 mM ferricyanide and 0.1 mM NADH

c: at 3 mM ferricyanide and 0.1-1 mM NADH

d: data were obtained from Seo et al. (2014)

e: data were obtained from Seo et al. (2004)

Figure1a

Click here to download high resolution image

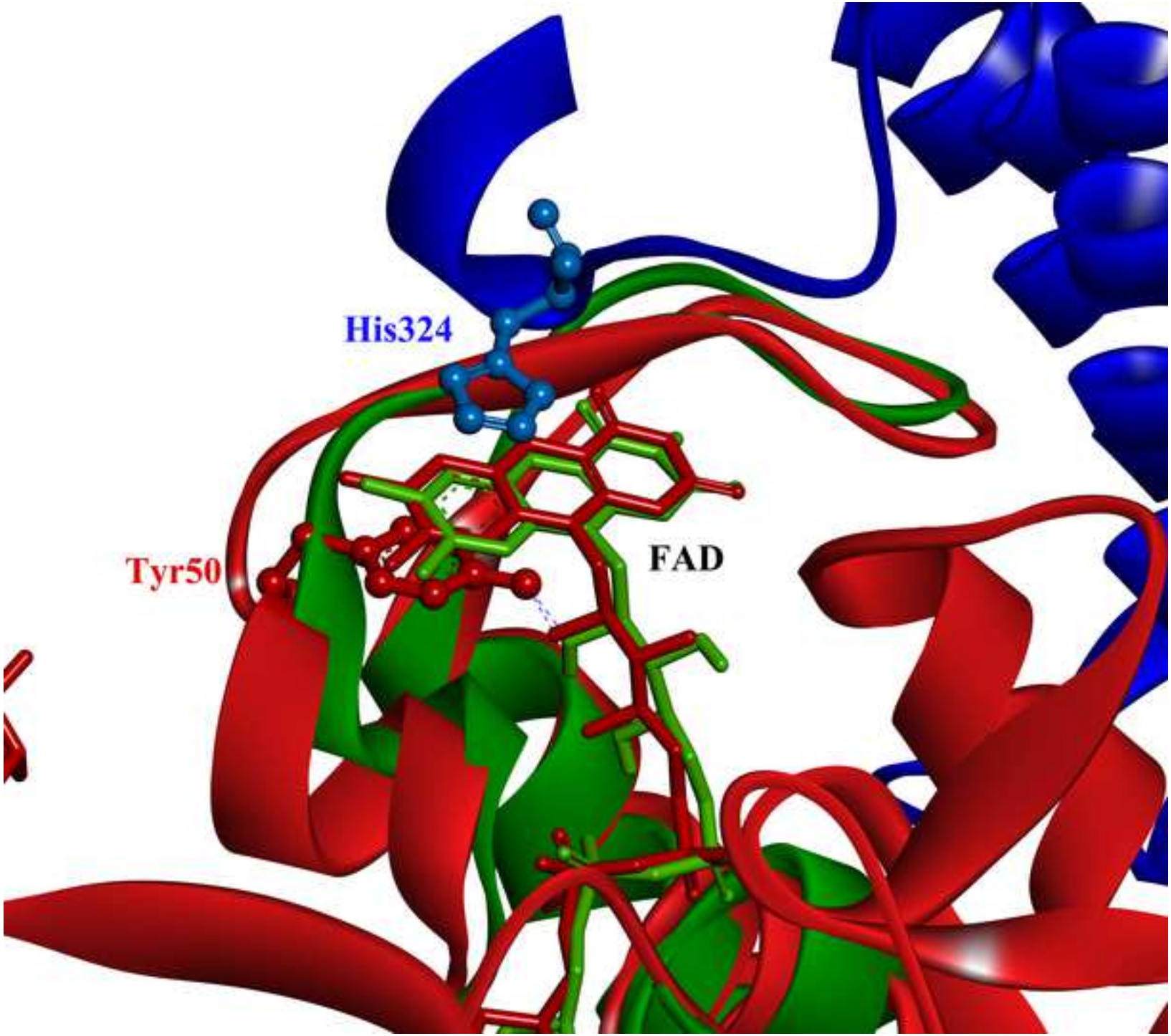

Figure1b
Click here to download Line figure: Figure 1b.eps

Figure 1B

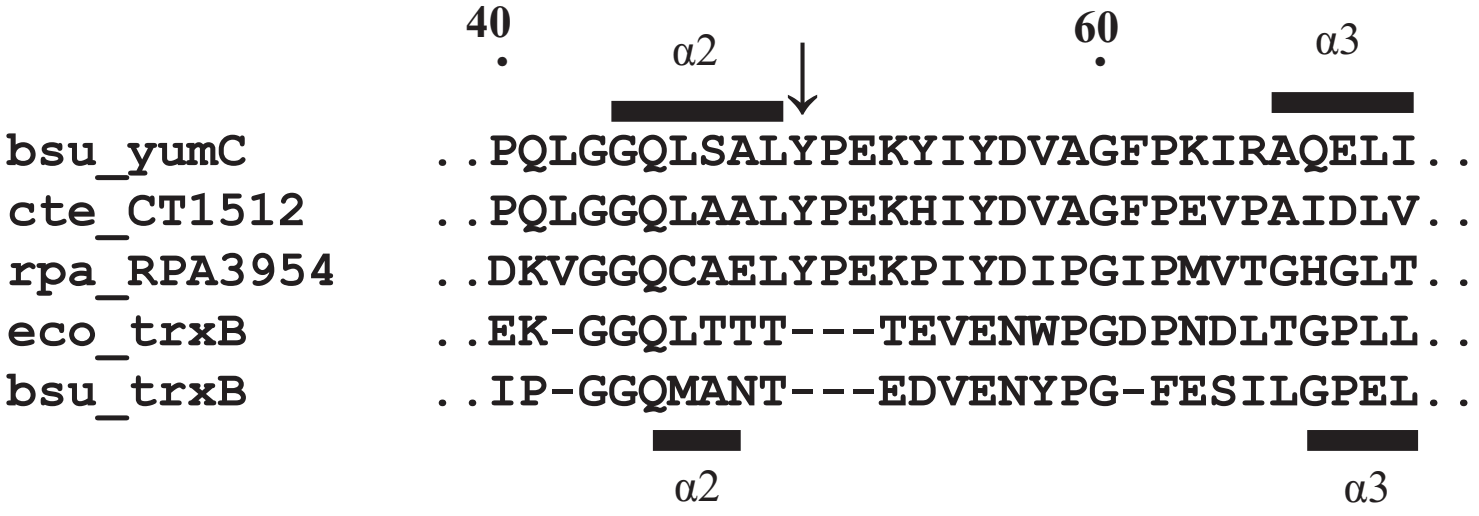

Figure 2a

Click here to download Line figure: Figure 2a.eps

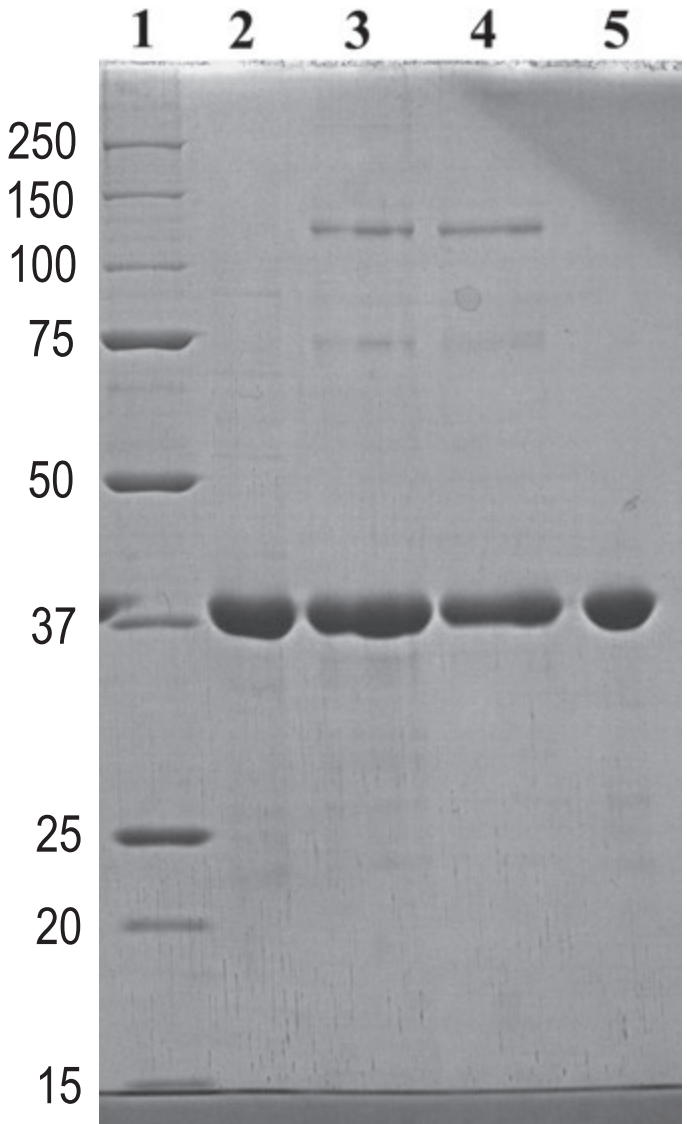

Figure2b
Click here to download Line figure: Figure 2b.eps

Figure 2b

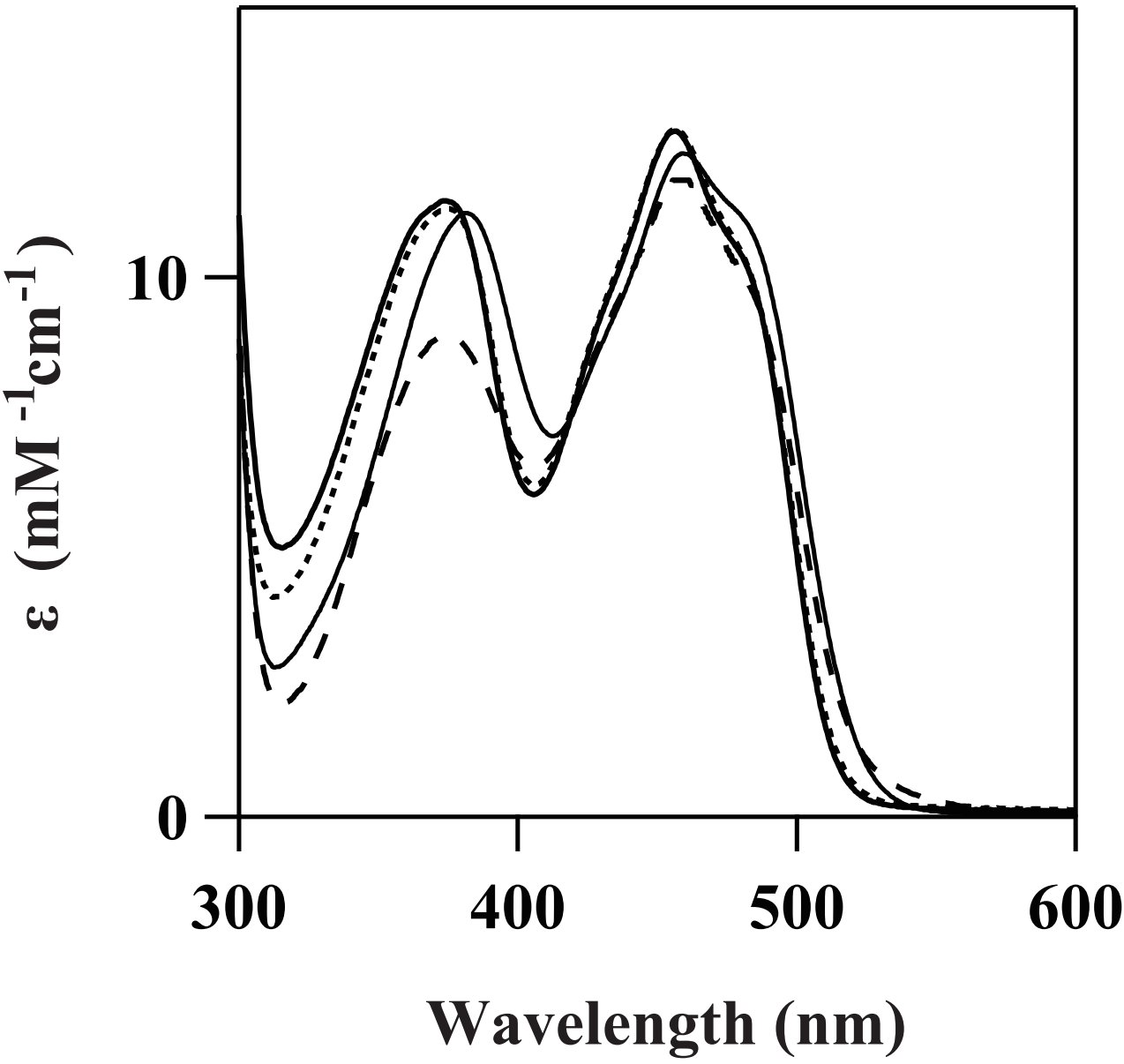

Figure2c

Click here to download Line figure: Figure 2c.eps

Figure 2c

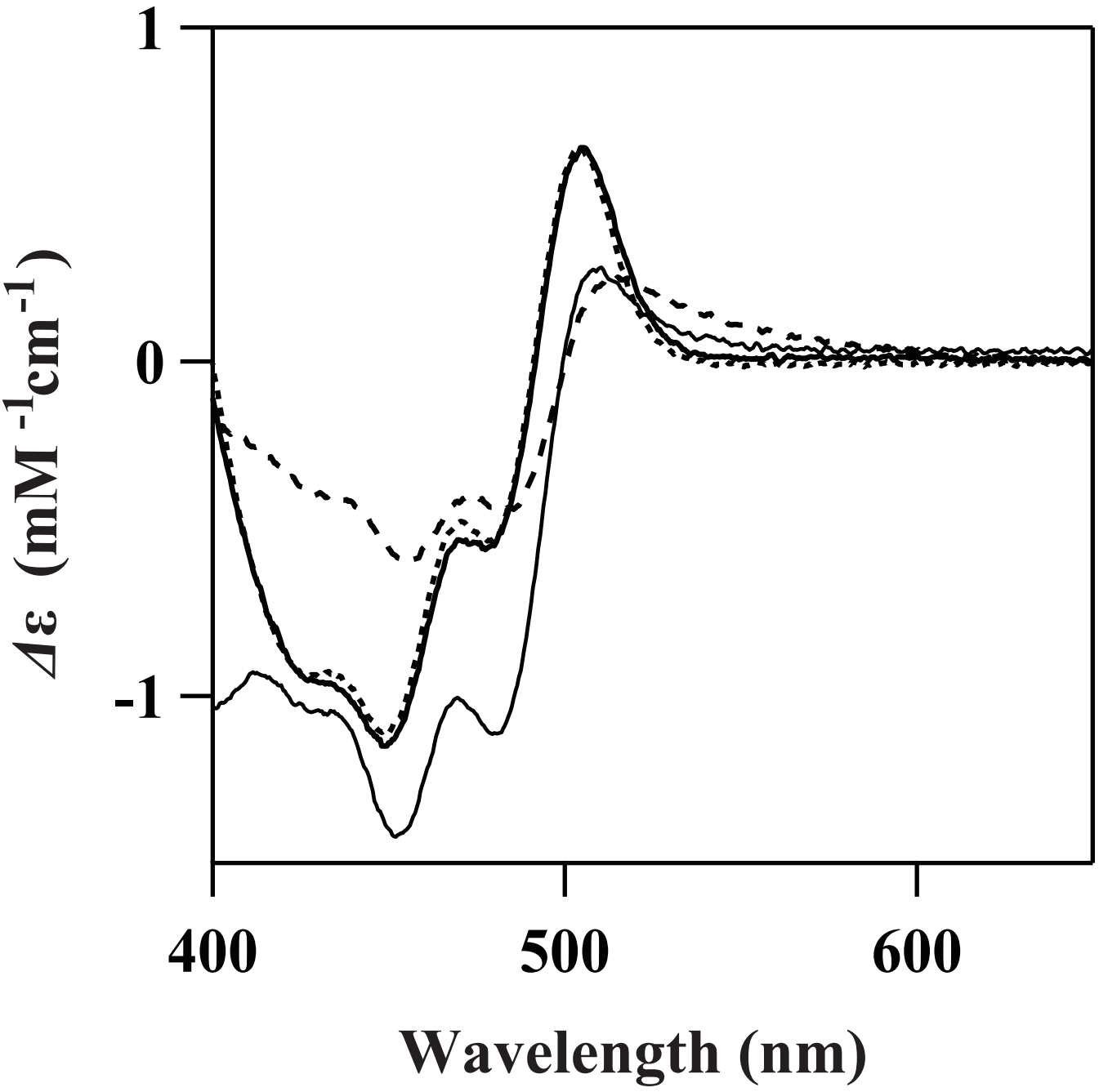

Figure 3a

Click here to download Line figure: Figure 3a.eps

Figure 3a

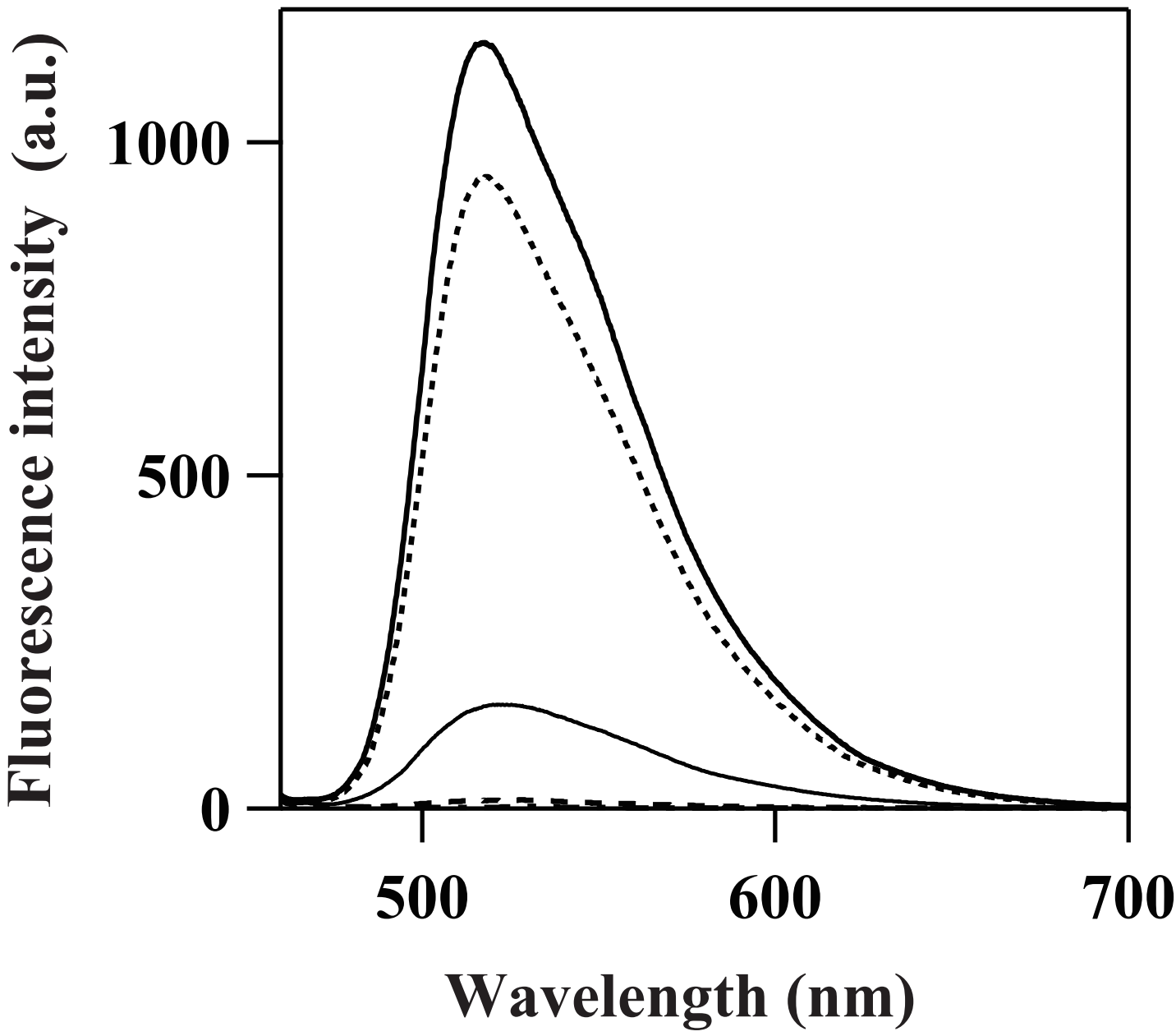

Figure 3b

Figure 3b

Click here to download Line figure: Figure 3b.eps

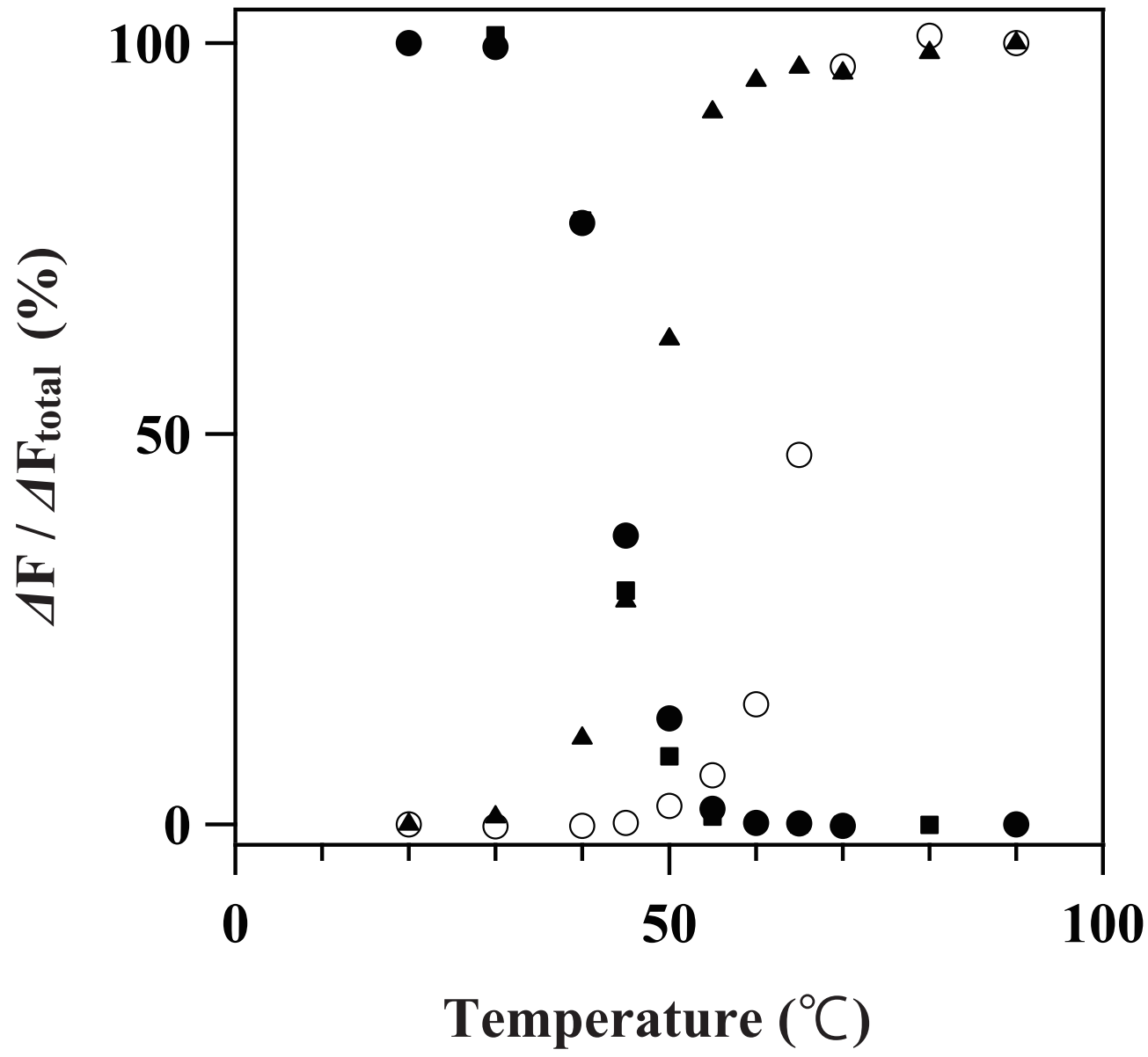

Figure4
Click here to download Line figure: Figure 4.eps

Figure 4